

Interaction of a Poincaré beam with optically polarized atoms in the presence of constant magnetic field

S. Ramakrishna^{1,2,3,*} and S. Fritzsche^{1,2,3}

¹*Helmholtz-Institut Jena, D-07743 Jena, Germany*

²*GSI Helmholtzzentrum für Schwerionenforschung GmbH, D-64291 Darmstadt, Germany*

³*Theoretisch-Physikalisches Institut, Friedrich-Schiller-Universität Jena, D-07743 Jena, Germany*
(Dated: March 25, 2025)

Recent studies have highlighted the frequent applications of structured light modes in optically pumped atomic magnetometers. In this work, we theoretically explore how a Poincaré beam probes an optically polarized atomic medium. Specifically, we consider atoms polarized by a plane wave with linear polarization, immersed in a constant external magnetic field. We analyze how the polarization of the pump and probe light fields, along with the external magnetic field, impact the absorption profile. To this end, we employ a density matrix approach based on the Liouville-von Neumann equation. Our results reveal that the absorption profile exhibits an asymmetric pattern that depends on the magnetic field strength and the mutual orientation of the pump and probe light propagation directions relative to the quantization axis. For illustration, we assume the incoming radiation drives an electric dipole transition, $5s^2S_{1/2} (F = 1) \rightarrow 5p^2P_{3/2} (F = 0)$, in rubidium atoms subjected to a magnetic field. These findings may aid in designing future experiments on optically pumped atomic magnetometers utilizing structured light modes.

I. INTRODUCTION

Optically pumped atomic magnetometers can be used to detect magnetic fields by monitoring properties such as intensity or polarization of the light at room temperatures [1]. This detection scheme has found significant applications in fields such as geophysics [2], medicine [3], and fundamental physics [4]. As a result, their use is steadily increasing compared to superconducting quantum interference devices, which need to be operated at cryogenic temperatures [5]. Additionally, notable progress has been made in developing compact and miniaturized atomic magnetometers [6].

Traditional atomic magnetometers rely on light fields with uniform polarization across their beam cross-section. However, modern optical techniques have enabled the generation of light fields with spatially varying polarization profiles [7]. One prominent member of this class of light fields is known as vector light modes. These light modes contain spatially variable linear polarization states within their beam cross-section [8]. Moreover, vector light beams have been shown to excite locally varying magnetization profiles in atoms, which can be utilized for measuring both static and oscillating magnetic field components [9–13]. In addition, an evolved version of vector beams, known as Poincaré beams, can also be generated [14, 15]. These beams exhibit a richer polarization texture across their beam cross-section [16]. Beyond vector light beams, a recent experiment demonstrated the elimination of dead-zones in an atomic magnetometer successfully with the help of a Poincaré beam [17].

Atomic magnetometers can have either single- or dual-beam configurations. While the single-beam configura-

tion favors the design of compact magnetometers, the dual-beam setup provides higher sensitivity in the measurement of magnetic fields [18, 19]. Recent experimental studies have demonstrated dual-beam atomic magnetometer schemes that are both compact and highly sensitive [20]. Within this dual-beam atomic magnetometer scheme, here we discuss the possibility of using a Poincaré beam to probe the response of polarized atomic medium to a constant magnetic field. To realize our aim, we analyze the dependence of absorption profile of a Poincaré beam on the parameters of both pump and probe light fields as well as the strength of the external magnetic field.

Initially, we discuss the interaction between a Poincaré beam and an unpolarized atomic target in the presence of a constant magnetic field. Subsequently, we utilize this knowledge to understand the interaction between Poincaré beam and a polarized atomic target. From these analysis, we found that the absorption profile of the Poincaré beam does not have axial symmetry unlike in the case of a vector beam. Moreover, this asymmetric absorption profile depends on the mutual orientation of the pump and probe light propagation directions relative to the quantization axis. We also discuss the dependence of the asymmetric absorption profile on the strength of the magnetic field. To illustrate these findings, we assume that the incoming radiation drives an electric dipole transition, $5s^2S_{1/2} (F = 1) - 5p^2P_{3/2} (F = 0)$, in the target Rb atoms subject to a constant magnetic field. We believe our results can be useful in guiding the future experiments of optically pumped atomic magnetometers utilizing structured light modes.

This paper is structured as follows: A brief mathematical description of a linearly polarized plane wave and Poincaré beam in Bessel basis is provided in Sec. II A. In Sec. II B, we derive the required transition amplitude of the interaction between the pump and probe light

* shreyas.ramakrishna@uni-jena.de

field with the atomic target. To determine the effect of the applied magnetic field on the absorption profile of a Poincaré beam, we employ density matrix theory, whose basic formulas are briefly reviewed in Sec. II C. In Sec. III A, we first discuss the absorption profile of the Poincaré beams interacting with unpolarized atomic target. As a next step, we discuss the absorption profile of Poincaré beams in the case of polarized atomic target, in Sec. III B. Finally, in Sec. IV we provide a brief summary and outlook.

II. THEORETICAL BACKGROUND

A. Pump and Probe light fields

1. Plane waves

In the current work, we consider the pump light field to be a linearly polarized plane wave. The vector potential of this plane wave, which is linearly polarized along the $x^{(\text{pump})}$ axis, see Fig. 2 and can be expressed as

$$\mathbf{A}_x^{(\text{lin})}(\mathbf{r}) = \frac{1}{\sqrt{2}} \left[\mathbf{A}_{\lambda=+1}^{(\text{circ})}(\mathbf{r}) + \mathbf{A}_{\lambda=-1}^{(\text{circ})}(\mathbf{r}) \right], \quad (1)$$

where $\mathbf{A}_\lambda^{(\text{circ})}(\mathbf{r})$ is the vector potential of a circularly polarized plane wave with helicity $\lambda = \pm 1$, given by

$$\mathbf{A}_\lambda^{(\text{circ})}(\mathbf{r}) = A_0 \mathbf{e}_{\mathbf{k}\lambda} e^{i\mathbf{k}\cdot\mathbf{r}}. \quad (2)$$

Here, \mathbf{k} is the propagation vector, and A_0 is the amplitude, whose value will be specified later.

2. Poincaré beams

In principle, a Poincaré beam can be constructed as a superposition of two or more circularly polarized structured light modes. In experiments, this is typically achieved by employing circularly polarized Laguerre-Gaussian (LG) modes. Theoretically, the observed physical properties near the beam center of these paraxial light fields can be reproduced using Bessel modes [21]. Thus, in our work, we construct the Poincaré beam in the Bessel basis, and the corresponding vector potential can be written as

$$\mathbf{A}^{(\text{poin})}(\mathbf{r}) = \frac{1}{\sqrt{2}} \left[\mathbf{A}_{m_\gamma=+1, \lambda=+1}^{(\text{B})}(\mathbf{r}) - \mathbf{A}_{m_\gamma=0, \lambda=-1}^{(\text{B})}(\mathbf{r}) \right]. \quad (3)$$

Here, $\mathbf{A}_{m_\gamma, \lambda}^{(\text{B})}(\mathbf{r})$ is the vector potential of circularly polarized Bessel light field carrying a projection of total angular momentum m_γ onto its propagation axis. Since the theory of Bessel light fields has been frequently discussed in past publications [22, 23], we will limit ourselves to the basic expressions. In particular, the vector potential

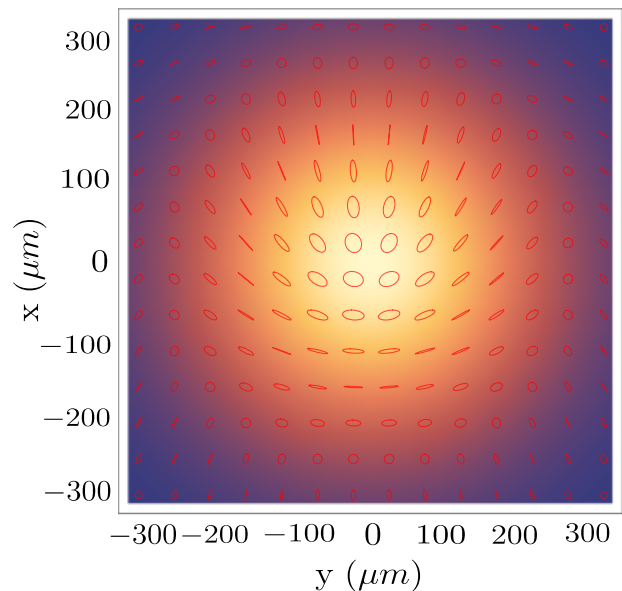


FIG. 1. The intensity and polarization profile of a Poincaré beam of wavelength 789 nm constructed using the Bessel light of opening angle $\theta_k = 0.05^\circ$.

of a circularly polarized Bessel light field can be written as

$$\mathbf{A}_{m_\gamma, \lambda}^{(\text{B})}(\mathbf{r}) = A_0 \int \frac{d^2 \mathbf{k}_\perp}{(2\pi)^2} a_{\varkappa m_\gamma}(\mathbf{k}_\perp) \mathbf{e}_{\mathbf{k}\lambda} e^{i\mathbf{k}\cdot\mathbf{r}}, \quad (4)$$

where $a_{\varkappa m_\gamma}(\mathbf{k}_\perp)$ is a weight function given by

$$a_{\varkappa m_\gamma}(\mathbf{k}_\perp) = \frac{2\pi}{\varkappa} (-i)^{m_\gamma} e^{im_\gamma \phi_k} \delta(\mathbf{k}_\perp - \varkappa). \quad (5)$$

From the above expressions, one can understand Bessel light field as superposition of plane waves in momentum space whose wave vectors $\mathbf{k} = (k_\perp, k_z)$ lie on the surface of a cone with an opening angle of $\theta_k = \arctan(\varkappa/k_z)$. By choosing smaller opening angle θ_k , one can obtain paraxial Bessel light fields in which the transverse momentum is much weaker than its longitudinal counterpart, that is, $\varkappa \ll k_z$ (see Ref. [23]). By using this condition, one can approximate the vector potential of a Poincaré beam (3) as

$$\begin{aligned} \mathbf{A}^{(\text{poin})}(\mathbf{r}, t) \approx & A_0 \left[-i \left\{ J_0(\varkappa r_\perp) + J_1(\varkappa r_\perp) e^{i\phi_r} \right\} \mathbf{e}_x \right. \\ & \left. + \left\{ J_0(\varkappa r_\perp) - J_1(\varkappa r_\perp) e^{i\phi_r} \right\} \mathbf{e}_y \right] e^{ik_z z} e^{i\omega t}. \end{aligned} \quad (6)$$

From this vector potential (6), we can obtain the electric field of a Poincaré beam using the relation $\mathbf{E}(\mathbf{r}, t) = \partial_t \mathbf{A}(\mathbf{r}, t)$. This can be further utilized to understand its transverse intensity and the polarization profile. While the transverse intensity of Poincaré beam resembles that of a Gaussian, it carries a rich polarization profile as shown in Fig. 1. In particular, the local state of polarization transitions from a (pure) circular near the beam center to elliptical polarization as we move away from the center, as shown in Fig. 1.

B. Transition amplitudes

Following the discussion of the mathematical formulation of pump and probe light fields, we now proceed to derive transition amplitude for the light atom interaction process. In particular, we will consider atomic transition from the initial $|\alpha_g F_g M_g\rangle$ to final $|\alpha_e F_e M_e\rangle$ atomic state driven by the incoming laser in the presence of external magnetic field $\mathbf{B}_{(\text{const})} = (0, 0, B_{(\text{const})})$. Moreover, this external constant magnetic field is chosen as the quantization axis of the total system through out this paper. Then, one could write the first order transition matrix

element as

$$V_{eg} = ec \left\langle \alpha_e F_e M_e \left| \sum_q \boldsymbol{\alpha}_q \cdot \mathbf{A}(\mathbf{r}_q) \right| \alpha_g F_g M_g \right\rangle, \quad (7)$$

with $\mathbf{F} = \mathbf{I} + \mathbf{J}$, where \mathbf{I} and \mathbf{J} are the nuclear and electron angular momenta, respectively, M is the projection of \mathbf{F} on the quantization axis, α denotes all additional quantum numbers required to specify the state uniquely, e is the elementary charge, and c is the speed of light. Moreover, q runs over all electrons in a target atom and $\boldsymbol{\alpha}_q$ denotes the vector of Dirac matrices for the q th particle [24]. In the above transition amplitude (7), $\mathbf{A}(\mathbf{r})$ denotes the vector potential of either pump or probe light field. Before proceeding further, it can be noted that the transition matrix elements for the interaction process between linearly polarized plane wave, and a Poincaré beam with atom can be constructed in a similar way to their respective vector potentials.

The transition amplitudes for a circularly polarized plane wave of helicity $\lambda = \pm 1$ is given by

$$V_{eg}^{(\text{circ})}(\lambda) = A_0 ec \sqrt{2\pi} \sum_{L,p} i^L [L, F_g]^{1/2} (i\lambda)^p D_{\Delta M, \lambda}^L(-\pi, \theta_p, -\pi) \langle F_g M_g, L \Delta M | F_e M_e \rangle \quad (8)$$

$$\times (-1)^{I+F_g+L+J_e} \begin{Bmatrix} F_e & F_g & L \\ J_g & J_e & I \end{Bmatrix} \langle \alpha_e J_e || \sum_q \boldsymbol{\alpha}_q \cdot \mathbf{a}_{L,q}^{(p)} || \alpha_g J_g \rangle,$$

and the transition amplitude for a Bessel light field with a given m_γ and $\lambda = \pm 1$ can be written as

$$V_{eg}^{(\text{B})}(m_\gamma, \lambda) = A_0 ec \sqrt{2\pi} \sum_M i^{L+M} [L, F_g]^{1/2} (i\lambda)^p (-1)^{m_\gamma} e^{i(m_\gamma - M)\phi_b} J_{m_\gamma - M}(\boldsymbol{\alpha} b) d_{M, \lambda}^L(\theta_k) \quad (9)$$

$$\times D_{\Delta M, M}^L(\pi, \theta_B, \pi) \langle F_g M_g, L \Delta M | F_e M_e \rangle (-1)^{I+F_g+L+J_e}$$

$$\times \begin{Bmatrix} F_e & F_g & L \\ J_g & J_e & I \end{Bmatrix} \langle \alpha_e J_e || \sum_q \boldsymbol{\alpha}_q \cdot \mathbf{a}_{L,q}^{(p)} || \alpha_g J_g \rangle.$$

In the above expressions, $\Delta M = M_e - M_g$, $[L, F_g] = (2L + 1)(2F_g + 1)$, $p = 1$ (or 0) denotes electric (or magnetic) atomic transition with a multipolarity L , $\langle \alpha_e J_e || \sum_q \boldsymbol{\alpha}_q \cdot \mathbf{a}_{L,q}^{(p)} || \alpha_g J_g \rangle$ is the reduced matrix elements, and $D_{\Delta M, \lambda}^L(\pi, \theta_B, \pi)$ is the Wigner D functions. Here, the arguments of the Wigner D functions are Euler angles that characterize the rotation from the atomic frame with the quantization axis along the magnetic field $\mathbf{B}_{\text{const}}$ to the photon frame with the quantization axis along the respective wave vectors \mathbf{k} [25]. Moreover, the angle $\theta_p = \pi - \theta_B$ ensures that at all the given times the pump and probe light fields are propagating perpendicular to each other, as shown in Fig. 2. Furthermore, taking into account the fact that Poincaré beam has a complex spatial structure, we have introduced impact parameter $\mathbf{b} = (b \cos \phi_b, b \sin \phi_b, 0)$ in (9) which will characterize the position of the atom within its beam cross-section [23].

One can write the transition amplitude for linearly po-

larized pump light field interacting with atomic target as

$$V_{eg,x}^{(\text{lin})} = \frac{1}{\sqrt{2}} \left[V_{eg}^{(\text{circ})}(\lambda = +1) + V_{eg}^{(\text{circ})}(\lambda = -1) \right]. \quad (10)$$

Similarly, the transition amplitude for the probe Poincaré beam can be written as

$$V_{eg}^{(\text{poin})} = \frac{1}{\sqrt{2}} \left[V_{eg}^{(\text{B})}(m_\gamma = +1, \lambda = +1) \quad (11)$$

$$- V_{eg}^{(\text{B})}(m_\gamma = 0, \lambda = -1) \right].$$

It should be noted that, vector potential of (non-paraxial) Bessel light (4) was used to derive the transition amplitude for the Poincaré beam atom interaction and this holds true for any arbitrary opening angle θ_k . That being said, we will restrict ourselves to smaller θ_k values in our calculation to remain within paraxial regime.

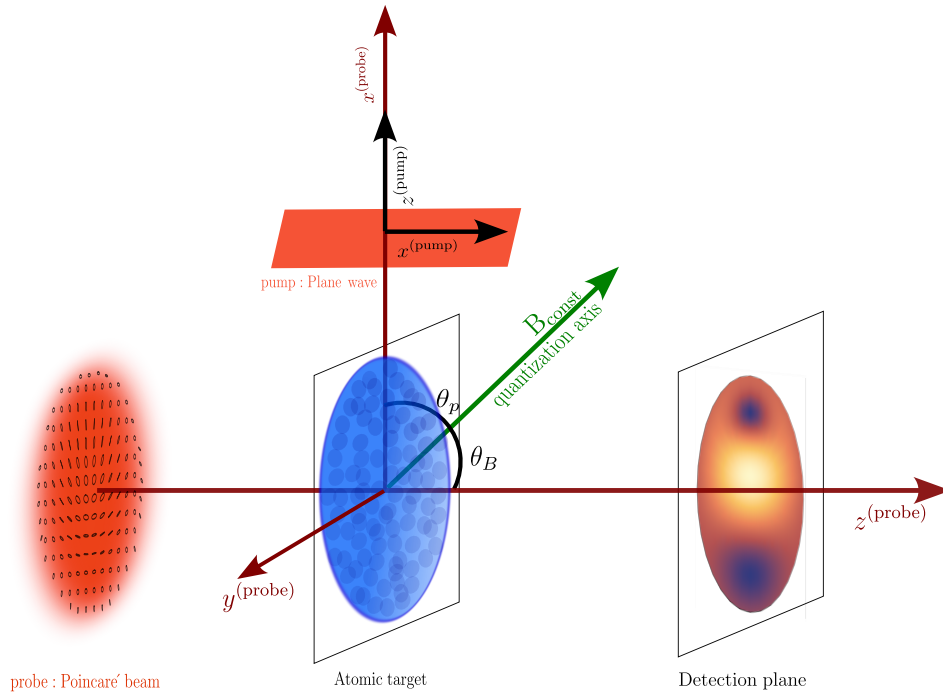


FIG. 2. Geometry of the proposed pump-probe atomic magnetometer setup. The atomic target interacts with a pump and a probe light propagating perpendicular to each other along $z^{(\text{pump})}$ and $z^{(\text{probe})}$, respectively. The pump, plane wave is linearly polarized along the $x^{(\text{pump})}$ direction and the probe, Poincaré beam has complex polarization texture. The external magnetic field, $\mathbf{B}_{\text{const}}$, is applied at an angle of θ_B with respect to the probe light field. The quantization axis of this system is chosen along the applied constant magnetic field.

C. Density matrix formalism

To theoretically model the time evolution of the atomic states interacting with both pump and probe light fields in the presence of external magnetic field, we here use Liouville-von Neumann equation [26]. In this approach, the state of a system is represented by the density operator $\hat{\rho}(t)$ and its time evolution is given by

$$\frac{d}{dt}\hat{\rho}(t) = -\frac{i}{\hbar}[\hat{H}(t), \hat{\rho}(t)] + \hat{R}(t). \quad (12)$$

Here $\hat{H}(t)$ is the total Hamiltonian of the atom in the presence of external fields, and $\hat{R}(t)$ is introduced to take into account phenomenologically spontaneous decay [27]. We consider transitions between the Zeeman sublevels of the ground $|\alpha_g F_g M_g\rangle$ to those of the excited state $|\alpha_e F_e M_e\rangle$, described by a density matrix of size $(2F_g + 2F_e + 2) \times (2F_g + 2F_e + 2)$. In this basis, we can write the elements of the density matrix as:

$$\rho_{gg'}(t) = \langle \alpha_g F_g M_g | \hat{\rho}(t) | \alpha_g F_g M_g' \rangle, \quad (13a)$$

$$\rho_{ee'}(t) = \langle \alpha_e F_e M_e | \hat{\rho}(t) | \alpha_e F_e M_e' \rangle, \quad (13b)$$

$$\rho_{ge}(t) = \langle \alpha_g F_g M_g | \hat{\rho}(t) | \alpha_e F_e M_e \rangle, \quad (13c)$$

$$\rho_{eg}(t) = \langle \alpha_e F_e M_e | \hat{\rho}(t) | \alpha_g F_g M_g \rangle. \quad (13d)$$

In Eqs. (13), the diagonal elements $\rho_{gg}(t)$ and $\rho_{ee}(t)$ are the probabilities of finding an atom in the Zeeman substates $|\alpha_g F_g M_g\rangle$ and $|\alpha_e F_e M_e\rangle$, whereas the off-diagonal elements describe the coherence between them.

In its matrix form the Liouville-von Neumann equation (12) represents a system of coupled differential equations for the evolution of the density matrix elements $\rho_{gg'}(t)$, $\rho_{ee'}(t)$, $\rho_{ge}(t)$, and $\rho_{eg}(t)$. To solve these equations, we introduce $\tilde{\rho}_{gg'}(t) = \rho_{gg'}(t)$, $\tilde{\rho}_{ee'}(t) = \rho_{ee'}(t)$, $\tilde{\rho}_{ge}(t) = \rho_{ge}(t)e^{-i\omega t}$, $\tilde{\rho}_{eg}(t) = \rho_{eg}(t)e^{i\omega t}$ and employ the rotating-wave approximation, which is valid when the angular frequency of the light field ω is sufficiently close to resonance [27, 28]. This approximation allows us to eliminate the fast-oscillating terms proportional to $e^{\pm 2i\omega t}$. It should be noted here that, in the current work we will assume the pump and probe light fields to have the same angular frequency ω . Following these conditions, the Liouville-von Neumann equations can be re-written as:

$$\frac{d}{dt}\tilde{\rho}_{gg'}(t; M_g, M_e) = -i\Omega_g^{(L)} [M_g - M'_g] \tilde{\rho}_{gg'}(t) - \frac{i}{2\hbar} \left[\sum_{M_e} V_{eg}^* \tilde{\rho}_{eg'}(t) - \sum_{M_e} V_{eg'} \tilde{\rho}_{ge}(t) \right] + R_{gg'}(t), \quad (14a)$$

$$\frac{d}{dt}\tilde{\rho}_{ee'}(t; M_g, M_e) = -i\Omega_e^{(L)} [M_e - M'_e] \tilde{\rho}_{ee'}(t) - \frac{i}{2\hbar} \left[\sum_{M_g} V_{eg} \tilde{\rho}_{ge'}(t) - \sum_{M_g} V_{e'g}^* \tilde{\rho}_{eg}(t) \right] + R_{ee'}(t), \quad (14b)$$

$$\frac{d}{dt}\tilde{\rho}_{ge}(t; M_g, M_e) = -i\Delta\tilde{\rho}_{ge}(t) + i \left[\Omega_e^{(L)} M_e - \Omega_g^{(L)} M_g \right] \tilde{\rho}_{ge}(t) - \frac{i}{2\hbar} \left[\sum_{M'_e} V_{e'g}^* \tilde{\rho}_{e'e}(t) - \sum_{M'_g} V_{eg'}^* \tilde{\rho}_{gg'}(t) \right] + R_{ge}(t), \quad (14c)$$

$$\frac{d}{dt}\tilde{\rho}_{eg}(t; M_g, M_e) = i\Delta\tilde{\rho}_{eg}(t) - i \left[\Omega_e^{(L)} M_e - \Omega_g^{(L)} M_g \right] \tilde{\rho}_{eg}(t) - \frac{i}{2\hbar} \left[\sum_{M'_g} V_{eg'} \tilde{\rho}_{g'g}(t) - \sum_{M'_e} V_{e'g} \tilde{\rho}_{ee'}(t) \right] + R_{eg}(t). \quad (14d)$$

In the above expressions, the $V_{eg} = V_{eg}^{(\text{pump})} + V_{eg}^{(\text{probe})}$ is the transition matrix element which is proportional to Rabi frequency, $\Delta = \omega - \omega_0$ denotes the light frequency detuning from resonance, ω_0 is the atomic transition frequency in the absence of external fields and $\Omega^{(L)} = g_F \mu_B B_{\text{const}} / \hbar$ is the Larmor frequency. The contribution of spontaneous decay to the $R(t)$ terms, obtained from the rate for emission summed over polarizations and integrated over angles, is

$$R_{gg'}(t) = \Gamma[F_g, J_e] \left\{ \begin{matrix} F_e & F_g & L \\ J_g & J_e & I \end{matrix} \right\}^2 \times \sum_{M_e, M'_e, M} \langle F_g M_g LM | F_e M_e \rangle \tilde{\rho}_{ee'}(t) \langle F_g M'_g LM | F_e M'_e \rangle, \quad (15a)$$

$$R_{ee'}(t) = -\Gamma[F_g, J_e] \left\{ \begin{matrix} F_e & F_g & L \\ J_g & J_e & I \end{matrix} \right\}^2 \tilde{\rho}_{ee'}(t), \quad (15b)$$

$$R_{ge}(t) = -\frac{1}{2}\Gamma[F_g, J_e] \left\{ \begin{matrix} F_e & F_g & L \\ J_g & J_e & I \end{matrix} \right\}^2 \tilde{\rho}_{ge}(t), \quad (15c)$$

$$R_{eg}(t) = -\frac{1}{2}\Gamma[F_g, J_e] \left\{ \begin{matrix} F_e & F_g & L \\ J_g & J_e & I \end{matrix} \right\}^2 \tilde{\rho}_{eg}(t), \quad (15d)$$

where Γ is the decay rate of the upper level $|\alpha_e J_e\rangle$ [13, 29, 30].

III. RESULTS AND DISCUSSION

In the present work, we investigate the interaction between a Poincaré beam and atoms in the presence of an external magnetic field. In experiments related to atomic magnetometers, this interaction between the probe light and atoms is quantified by detecting the absorption profile of the transmitted light. Specifically, the absorption profile reveals which parts of the beam cross-section were

absorbed by the interacting atoms. Theoretically, this can be examined by monitoring the populations of the excited and ground states of the atoms across the beam cross-section. This approach was outlined in an earlier publication [13] and is equivalent to calculating the imaginary part of the refractive index of the polarized atomic medium.

The theoretical framework developed in the previous section can be used to analyze atomic transitions between any two hyperfine levels of a given atomic system. However, in this work, we consider an electric dipole transition between $5s \ ^2S_{1/2}$ ($F = 1$) and $5p \ ^2P_{3/2}$ ($F = 0$) in a Rb atom, driven by a laser with frequency $\omega = \omega_0 = 2\pi \times 384$ THz at zero detuning, as assumed earlier. Furthermore, we set the amplitude of the pump light field to $A_0 = 1.28 \times 10^{-13}$ and that of the probe light beam to $A_0 = 2.02 \times 10^{-14}$. Additionally, the Bessel mode used to construct the Poincaré beam is assigned an opening angle of $\theta_k = 0.05^\circ$. These parameters correspond to experimentally realistic pump (Gaussian) and probe (Poincaré) light fields in the LG basis with a beam waist of approximately $300 \mu\text{m}$. Moreover, we assume the power of the pump light field to be ten times higher than that of the probe, as is commonly done in experiments [12].

Along with these beam parameters, we require the values of the spontaneous decay rate Γ and the reduced matrix element $\langle \alpha_e J_e || \sum_q \alpha_q \cdot \mathbf{a}_{L,q}^{(p)} || \alpha_g J_g \rangle$. The spontaneous decay rate, $\Gamma = 4.042 \times 10^7 \text{ s}^{-1}$, is obtained from the JAC code [31], which can be further used to calculate the reduced matrix element.

A. Unpolarized atomic target

Let us begin our discussion by considering the interaction of a Poincaré beam with a unpolarized atomic target, meaning the pump light field is turned off. In this simpli-

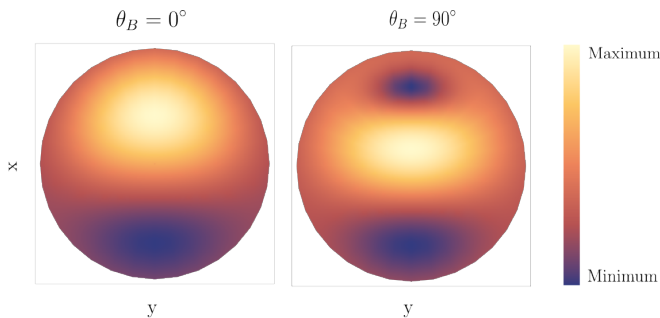


FIG. 3. Absorption profile of the Poincaré beam for a unpolarized rubidium atomic target immersed in an external constant magnetic field. Here, the Poincaré beam is propagating at an angle of $\theta_B = 0^\circ$ and 90° with respect to the applied magnetic field of strength $B_{(\text{const})} = 1$ G. In this absorption profile, maximum parts corresponds to higher number of atoms in the excited state.

fied scenario, we examine the population of the excited atomic state across the beam cross-section under steady-state conditions in presence of an external magnetic field of $B_{(\text{const})} = 1$ G. This is later used to construct the absorption profile. For clarity, we focus on two cases: (a) Poincaré probe field propagating parallel ($\theta_B = 0^\circ$) and (b) perpendicular (90°) to the quantization axis. As shown in Fig. 3, the absorption profile exhibits asymmetry along the y -axis in both cases.

1. For $\theta_B = 0^\circ$

In particular, when the angle $\theta_B = 0^\circ$, the atoms present in the upper half of the beam cross-section absorb more light than those in the lower half. This imbalance in absorption arises from the asymmetry in the polarization profile of the Poincaré beam. Specifically, the Poincaré beam exhibits an asymmetric polarization distribution with respect to the y -axis (see Fig. 1). This asymmetry in the polarization profile of the light field affects the local transition amplitude, as shown in upper panel of Fig. 4. These figures depict the polar plot of the absolute transition amplitude $|V_{eg}^{(\text{poin})}|$ of Poincaré beam interacting with atoms located at a radial distance of $b = 200 \mu\text{m}$ from the beam center. Among these, the transition amplitude between the $M_g = \mp 1$ and $M_e = 0$ ($\Delta M = \pm 1$) magnetic sublevels is symmetric. However, the amplitude for the atomic transition between sublevels $M_g = 0$ and $M_e = 0$ ($\Delta M = 0$) is asymmetric with lower values in the bottom half, see upper panel of Fig. 4. Consequently, the absorption profile of the Poincaré beam is also asymmetric, as shown in Fig. 3, with reduced absorption in the lower half of the beam cross-section.

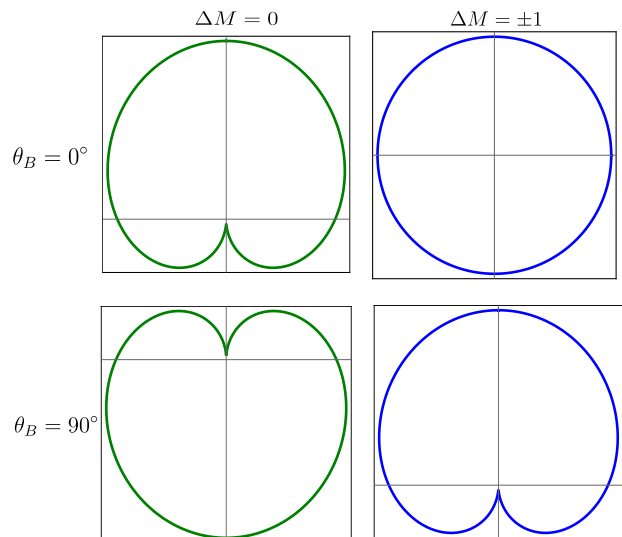


FIG. 4. Polar plots of absolute value of transition amplitude $V_{eg}^{(\text{poin})}$ between $M_g = 0$ to $M_e = 0$ ($\Delta M = 0$) and $M_g = \mp 1$ to $M_e = 0$ ($\Delta M = \pm 1$) for the Poincaré beam propagating at $\theta_B = 0^\circ$ and 90° . Here, the interacting rubidium atoms are assumed to be localised at $b = 200 \mu\text{m}$ from the beam axis and external magnetic field of $B_{(\text{const})} = 1$ G is applied.

2. For $\theta_B = 90^\circ$

In contrast to $\theta_B = 0^\circ$, the angle between the local polarization direction and the quantization axis varies across the beam cross-section when $\theta_B = 90^\circ$. Specifically, in the upper half of the beam cross-section, where the atoms are located near $\phi_b = 0^\circ$, the major axis of the local elliptically polarized light field aligns parallel to the quantization axis. Conversely, in the lower half, at $\phi_b = 180^\circ$, the major axis of the ellipse is oriented perpendicular to the quantization axis. This asymmetry influences the transition amplitude of the interaction between atoms and the Poincaré beam across the beam cross-section. This effect is evident in the polar plots of the absolute transition amplitude, where we have chosen the radial distance to be $b = 200 \mu\text{m}$. Notably, in this case, both the transition amplitudes for $\Delta M = 0$ and ± 1 exhibit asymmetry across the beam cross-section of the probe light, see bottom panel of Fig. 4. As a result, the absorption profile exhibits more pronounced asymmetry compared to the case of $\theta_B = 0^\circ$ as shown in Fig. 3.

In addition, from Fig. 3, it should be noted that the atoms positioned at $\mathbf{b} = 0$ absorb relatively more light for $\theta_B = 90^\circ$ than for 0° . This can be understood as follows: Near the beam center, the local state of polarization of the Poincaré beam is circular, (see Fig. 1). Because of this, for $\theta_B = 0^\circ$, atoms at $\mathbf{b} = 0$ undergo transitions only between the ground $M_g = -1$ and the excited magnetic sublevel $M_e = 0$. In contrast, for $\theta_B = 90^\circ$, the incoming light field can drive transitions between all the ground $M_g = 0, \mp 1$ and the excited $M_e = 0$ state, leading to a greater population of atoms in the excited state.

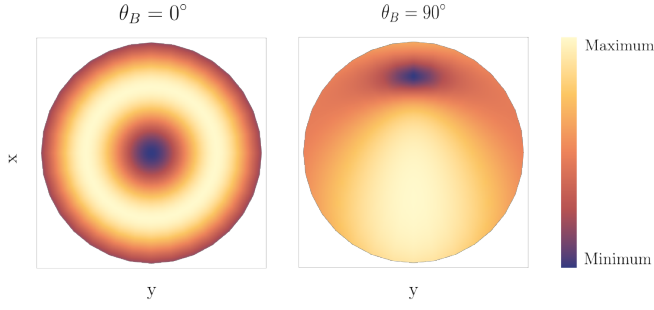


FIG. 5. Absorption profile of the Poincaré beam for a polarized rubidium atomic target immersed in an external constant magnetic field. Here, the Poincaré beam is propagating at an angle of $\theta_B = 0^\circ$ and 90° with respect to the applied magnetic field of strength $B_{(\text{const})} = 1$ G. In this absorption profile, maximum parts corresponds to higher number of atoms in the excited state.

B. Polarized atomic target

Now, we examine the interaction between the incoming Poincaré beam and optically polarized rubidium atoms subjected to a constant magnetic field of strength $B_{(\text{const})} = 1$ G. Similar to the previous case, we assume the Poincaré beam to propagate either parallel ($\theta_B = 0^\circ$) or perpendicular ($\theta_B = 90^\circ$) to the quantization axis. When $\theta_B = 0^\circ$, the pump light field propagates perpendicular to the quantization axis. This results in the polarization direction of the pump light field to be parallel to the quantization axis. In this configuration, the pump light field drives an atomic transition which satisfies the angular momentum selection rule $\Delta M = 0$, see Fig 6 (a). Moreover, this creates a polarized atomic medium with minimum population in the ground state $M_g = 0$.

1. For $\theta_B = 0^\circ$

In Fig. 5, we show the absorption profile at a steady-state condition for the Poincaré beam propagating at an angle of $\theta_B = 0^\circ$. For this scenario, the absorption profile displays a *donut-like* pattern. In comparison to the earlier case of unpolarized atomic target, here the absorption profile has an axial symmetry. This behavior can be understood by examining the transition matrix elements of the probe light-atom interaction process. In the upper panel of Fig. 4, we show the absolute value of the transition amplitudes for $\Delta M = 0, \pm 1$ in the beam cross-section, choosing the radial distance of $b = 200 \mu\text{m}$. From these plots, we observe that the asymmetry in the local polarization profile of the Poincaré beam only affects the amplitude $V_{eg}^{(\text{point})}$ for the transition $\Delta M = 0$. Since we consider a polarized atomic target which has minimum population in the ground state $M_g = 0$, the probability of probe light field driving transition with $\Delta M = 0$ is also minimized. Therefore, the Poincaré beam predominantly induces transition between the ground $M_g = \mp 1$

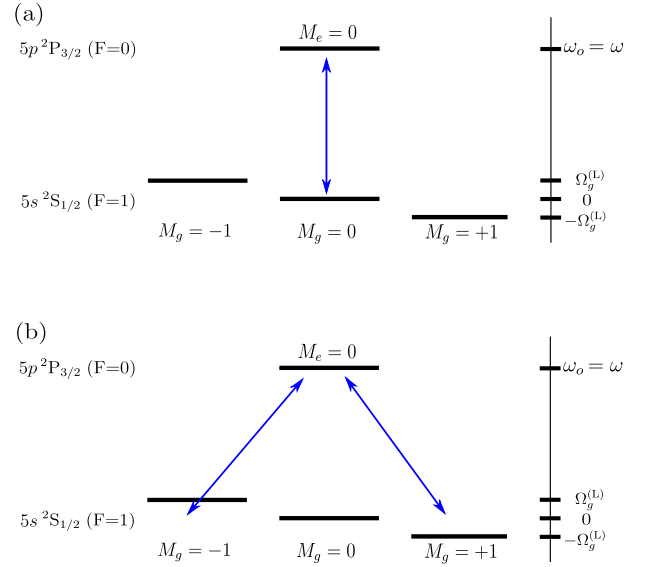


FIG. 6. The transition between $5s^2S_{1/2} (F=1) - 5p^2P_{3/2} (F=0)$ in ^{87}Rb driven by the pump, linearly polarized plane wave for (a) $\theta_B = 0^\circ$ and (b) $\theta_B = 90^\circ$. The lower sublevels are split by the energy $\hbar\Omega_g^{(L)}$ as given by the Larmor frequency of the atom in the magnetic field.

and excited state $M_e = 0$. As the amplitude $V_{eg}^{(\text{point})}$ for the transition $\Delta M = \pm 1$ possesses an axial symmetry, the absorption profile of the Poincaré beam for $\theta_B = 0^\circ$ does not exhibit any signs of asymmetry. In addition, this absorption profile exhibits a minimum near the beam center. Specifically, the atoms positioned near the beam center ($\mathbf{b} = 0$) absorbs less light, resulting in lower population of excited atoms. Furthermore, the atoms at the center interact with a local electric field that is circularly polarized, see Fig. 1. This suggests that the atoms near the center $\mathbf{b} = 0$ have higher probability to undergo a transition from ground $M_g = -1$ to $M_e = 0$ excited state. It should be noted that this particular atomic transition is relatively weaker than the transition driven by pump light field due to their respective power. Therefore, although the population of the excited atoms initially increases, it decreases steadily with time, eventually reaching a minimal constant value as the system approaches a steady-state condition, see Fig. 7. This change is also reflected in the dynamics of the ground level populations. In particular, the population of magnetic sublevels $M_g = -1, 0$ decreases over the time, while the population of $M_g = +1$ increases, with the system reaching a steady-state. This behavior is expected because the ground sublevel $M_g = +1$ of the atoms near the center $\mathbf{b} = 0$ is not coupled with any of the light fields. As one moves farther away from the beam center, the local state of polarization changes from a pure circular to elliptical. This leads to a situation where the atoms farther from the beam center to absorb more light. Hence, we notice an relative increase in the number of population of the atoms in the excited state in comparison to

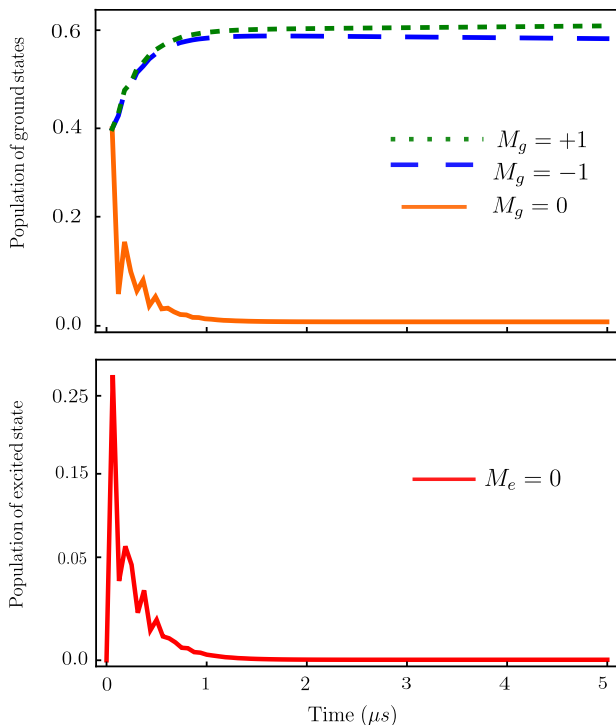


FIG. 7. Time evolution of the ground $5s \ ^2S_{1/2}$ ($F = 1$) and the excited $5p \ ^2P_{3/2}$ ($F = 0$) state populations of ^{87}Rb at the center of the beam cross-section $b = 0$. Here, the Poincaré beam propagating along the quantization axis ($\theta_B = 0^\circ$) interacts with a polarized Rb atoms exposed to a constant magnetic field of $B_{(\text{const})} = 1$ G.

the atoms at $\mathbf{b} = 0$.

2. For $\theta_B = 90^\circ$

Now, we consider the case where the Poincaré beam propagates at an angle of $\theta_B = 90^\circ$ with respect to the quantization axis. In this configuration, the pump, linearly polarized plane wave propagates along the quantization axis. In addition, here the quantization axis lies in the transverse plane of the probe light field. Under these conditions, the pump light field drives the transition in rubidium atom that satisfy the selection rule $\Delta M = \pm 1$, see Fig. 6 (b). Consequently, the population of the ground sublevel $M_g = 0$ exceeds that of the other two. The corresponding absorption profile of Poincaré beam at the steady-state condition is illustrated in Fig. 5. In contrast to the case $\theta_B = 0^\circ$, this absorption profile exhibits an asymmetrical pattern with respect to y -axis. This behavior arises due to the asymmetry in the local polarization distribution of the Poincaré beam. Unlike the scenario for $\theta_B = 0^\circ$, where polarization asymmetry affects only certain transitions, here, all three atomic transitions between the ground $M_g = 0, \pm 1$ and excited state $M_e = 0$ are affected by the asymmetrical polarization profile of the probe light field, see the bottom panel

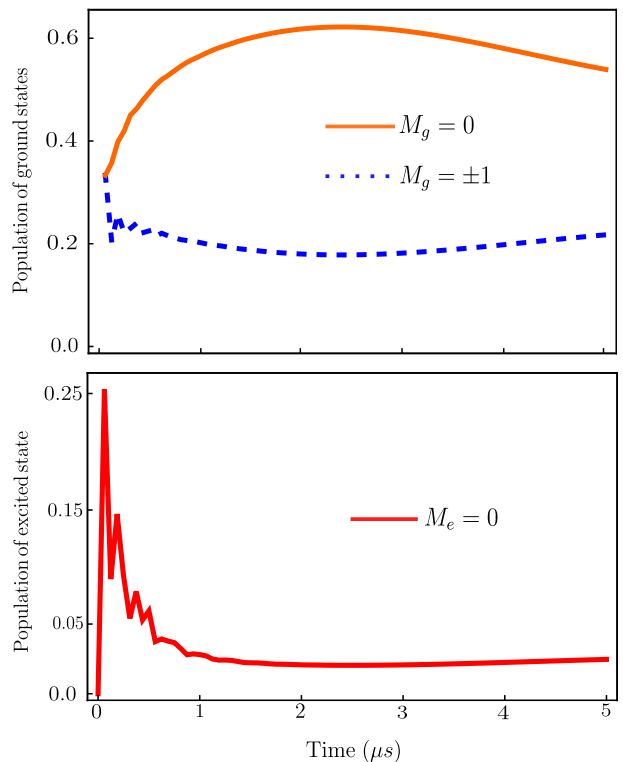


FIG. 8. Time evolution of the ground $5s \ ^2S_{1/2}$ ($F = 1$) and the excited $5p \ ^2P_{3/2}$ ($F = 0$) state populations of ^{87}Rb at the center of the beam cross-section $b = 0$. Here, the Poincaré beam propagating perpendicular to the quantization axis ($\theta_B = 90^\circ$) interacts with a polarized Rb atoms exposed to a constant magnetic field of $B_{(\text{const})} = 1$ G.

of Fig. 4. As a result, the absorption profile for $\theta_B = 90^\circ$ does not exhibit axial symmetry.

A key difference between $\theta_B = 90^\circ$ and 0° is that at $\mathbf{b} = 0$ more atoms populate the excited state, leading to greater light absorption. This occurs because the probe light now drives transitions from all the ground states to the excited state. This effect is evident in the time-evolution of the population of the ground states, as shown in Fig. 8. As the system reaches steady-state, population of ground sublevels $M_g = \pm 1$ decreases while $M_g = 0$ increases. Although the dynamics of the excited state population follows the same trend as before ($\theta_B = 0^\circ$), it reaches a higher steady-state value here. Additionally, the absorption profile in the present scenario exhibits a strong asymmetry with respect to the y axis, see Fig. 5. That is, more light is absorbed in the lower half of the beam cross-section in comparison to upper half. As explained earlier, this imbalance arises from the polarization structure of Poincaré beam.

Next, we examine how the absorption profile depends on the strength of the applied magnetic field $B_{(\text{const})}$. Fig. 9 presents both the absorption profile and its corresponding polar plots, which exhibit an *apple-like* pattern. This pattern represents the absorption intensity for atoms located at radial distance of $b = 200 \mu\text{m}$. We fo-

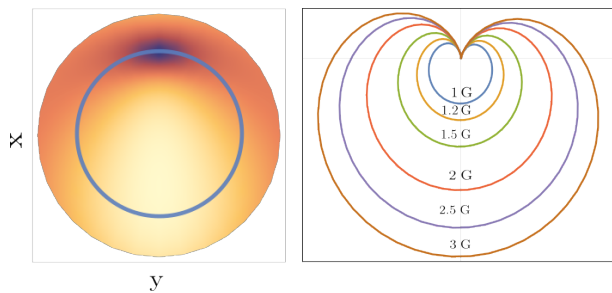


FIG. 9. Left: Absorption profile of the Poincaré beam propagating at ($\theta_B = 90^\circ$) interacting with a polarized rubidium atomic target immersed in an external constant magnetic field of $B_{(\text{const})} = 1$ G. Right: Polar plots of the absorption intensity corresponding to the radius ($b = 200 \mu\text{m}$) of circle shown in the adjacent absorption profile. These polar plots are shown for increasing magnetic field strengths.

cus on the case of angle $\theta_B = 90^\circ$, as this configuration results in an asymmetric absorption profile for the probe light. For simplicity, we vary the strength of the applied constant magnetic field from 1 to 3 Gauss. As shown in Fig. 9, the *apple-like* pattern expands as the magnetic field strength increases from 1 to 3 Gauss. Specifically, the absorption of the Poincaré beam in the lower half of the beam cross-section increases with the magnetic field strength. However, the imbalance in the absorption profile of the Poincaré beam persists regardless of increase in the magnetic field strength. This suggests that the absorption profile of the Poincaré beam at $\theta_B = 90^\circ$ can be used to determine the strength of the external magnetic field.

Based on this preliminary investigation, the proposed atomic magnetometer scheme can detect magnetic field strength as weak as $B_{(\text{const})} = 0.2$ G, see Fig. 9. However, further studies are needed to evaluate the sensitivity of our proposed atomic magnetometer for weaker magnetic fields.

IV. SUMMARY AND OUTLOOK

In this work, we analyzed the interaction between Poincaré beams and an optically polarized atomic target

in the presence of constant magnetic field. To conduct this analysis, we used a linearly polarized plane wave as the pump light and Poincaré beam as the probe light. Particularly, we used (paraxial) Bessel modes to construct the vector potential and the corresponding transition amplitude of the Poincaré beam interacting with the target atoms. This interaction process was studied with the help of Liouville-von Neumann equations.

We paid special attention to the population of the excited atomic state, which was later used to plot the absorption profile of the probe Poincaré beam. In particular, we examined this absorption profile both in the absence and presence of the pump light field for $\theta_B = 0^\circ$ and 90° , respectively. Our analysis show that the axial asymmetry present in the polarization profile of the Poincaré beam influences the local transition amplitude, thereby affecting the absorption profiles. Furthermore, we explored the potential application of using the proposed scheme in detecting the magnetic field strengths between 1 and 3 Gauss.

To simplify our theoretical calculations, we made the following assumptions: (a) thermal motion of atoms in the medium was neglected, (b) the pump and probe light fields were assumed to have same frequency, and (c) one-dimensional constant magnetic field was considered. In the forthcoming publication, we aim to extend this analysis of detecting constant magnetic field by incorporating the effects of atomic thermal motion and a time-dependent magnetic fields.

ACKNOWLEDGMENTS

We acknowledge support from the Research School of Advanced Photon Science of the Helmholtz Institute Jena.

-
- [1] edited by D. Budker and D. F. J. Kimball, *Optical Magnetometry* (Cambridge University Press, Cambridge, England, 2013).
 - [2] H. B. Dang, A. C. Maloof, and M. V. Romalis, *Appl. Phys. Lett.* **97**, 151110 (2010).
 - [3] C. N. Johnson, P. D. D. Schwindt, and M. Weisend, *Phys. Med. Biol.* **58**, 6065 (2013).
 - [4] G. Vasilakis, J. M. Brown, T. W. Kornack, and M. V. Romalis, *Phys. Rev. Lett.* **103**, 261801 (2009).
 - [5] D. Budker and M. Romalis, *Nat. Phys.* **3**, 227 (2007).
 - [6] V. Shah, S. Knappe, P. D. D. Schwindt, and J. Kitching, *Nat. Photonics* **1**, 649 (2007).
 - [7] H. Rubinsztein-Dunlop, A. Forbes, M. V. Berry, M. R. Dennis, D. L. Andrews, M. Mansuripur, C. Denz, C. Alpmann, P. Banzer, T. Bauer, E. Karimi, L. Marrucci, M. Padgett, M. Ritsch-Marte, N. M. Litchinitser, N. P. Bigelow, C. Rosales-Guzmán, A. Belmonte, J. P. Torres, T. W. Neely, M. Baker, R. Gordon, A. B. Stilgoe, J. Romero, A. G. White, R. Fickler, A. E. Willner, G. Xie, B. McMorran, and A. M. Weiner, *J. Opt.* **19**,

- 013001 (2017).
- [8] G. J. Gbur, *Singular optics* (CRC press, 2017).
- [9] F. Castellucci, T. W. Clark, A. Selyem, J. Wang, and S. Franke-Arnold, *Phys. Rev. Lett.* **127**, 233202 (2021).
- [10] S. Qiu, J. Wang, F. Castellucci, M. Cao, S. Zhang, T. W. Clark, S. Franke-Arnold, H. Gao, and F. Li, *Photon. Res.* **9**, 2325 (2021).
- [11] Y. Sun and Z. Wang, *Opt. Express* **31**, 15409 (2023).
- [12] G. Cai, K. Tian, and Z. Wang, *Laser & Photonics Reviews* **18**, 2400465 (2024).
- [13] S. Ramakrishna, R. P. Schmidt, A. A. Peshkov, S. Franke-Arnold, A. Surzhykov, and S. Fritzsche, *Phys. Rev. A* **110**, 043101 (2024).
- [14] J. A. Jones, A. J. D'Addario, B. L. Rojec, G. Milione, and E. J. Galvez, *American Journal of Physics* **84**, 822 (2016).
- [15] D. Li, S. Feng, S. Nie, C. Chang, J. Ma, and C. Yuan, *Journal of Applied Physics* **125**, 073105 (2019).
- [16] A. M. Beckley, T. G. Brown, and M. A. Alonso, *Opt. Express* **18**, 10777 (2010).
- [17] K. Tian, W. Ding, and Z. Wang, *Photon. Res.* **12**, 1093 (2024).
- [18] V. Shah, S. Knappe, P. D. D. Schwindt, and J. Kitching, *Nature Photonics* **1**, 649 (2007).
- [19] I. Savukov and M. G. Boshier, *Sensors* **16** (2016), 10.3390/s16101691.
- [20] B. Zhao, J. Tang, H. Yang, L. Li, Y. Zhang, Y. Liu, and Y. Zhai, *Optics & Laser Technology* **159**, 109025 (2023).
- [21] R. Lange, N. Huntemann, A. A. Peshkov, A. Surzhykov, and E. Peik, *Phys. Rev. Lett.* **129**, 253901 (2022).
- [22] O. Matula, A. G. Hayrapetyan, V. G. Serbo, A. Surzhykov, and S. Fritzsche, *J. Phys. B* **46**, 205002 (2013).
- [23] S. A.-L. Schulz, A. A. Peshkov, R. A. Müller, R. Lange, N. Huntemann, C. Tamm, E. Peik, and A. Surzhykov, *Phys. Rev. A* **102**, 012812 (2020).
- [24] W. R. Johnson, *Atomic Structure Theory* (Springer, New York, 2007).
- [25] M. E. Rose, *Elementary Theory of Angular Momentum* (John Wiley & Sons, New York, 1957).
- [26] K. Blum, *Density Matrix Theory and Applications* (Springer, Berlin, 2012).
- [27] M. Auzinsh, D. Budker, and S. M. Rochester, *Optically Polarized Atoms: Understanding Light-Atom Interactions* (Oxford University, Oxford, 2010).
- [28] L. von der Wense, P. V. Bilous, B. Seiferle, S. Stellmer, J. Weitenberg, P. G. Thirolf, A. Pálffy, and G. Kazakov, *Eur. Phys. J. A* **56**, 176 (2020).
- [29] P. Tremblay and C. Jacques, *Phys. Rev. A* **41**, 4989 (1990).
- [30] R. P. Schmidt, S. Ramakrishna, A. A. Peshkov, N. Huntemann, E. Peik, S. Fritzsche, and A. Surzhykov, *Phys. Rev. A* **109**, 033103 (2024).
- [31] S. Fritzsche, *Comput. Phys. Commun.* **240**, 1 (2019).